JMEMS Letters

MEMS Flow Sensor Using Suspended Graphene Diaphragm With Microhole Arrays

Qiugu Wang, Yifei Wang, and Liang Dong

***Abstract*— This letter reports a miniature flow sensor using a suspended composite membrane of graphene and silicon nitride containing an array of microscale through-holes. As a fluid flow passes through these microholes, the graphene layer of the composite membrane is stressed to change its electrical resistance due to the piezoresistive effect of graphene. The creation of the microholes in graphene allows for a wide dynamic range of the sensor from 5 to 56 m/s of air flow velocity. The sensor also exhibits an air flow rate sensitivity of $\sim 7 \times 10^{-8}$ $(m/s)^{-1}$. [2018-0133]**

***Index Terms*— MEMS, flow sensor, graphene.**

I. Introduction

FLOW rate measurement is crucial in many applications, such as environmental monitoring, process control and medical surveillance, where monitoring of fluid (including both gas and liquid) flow is needed. Many microelectromechanical systems (MEMS) flow sensors are compatible with semiconductor manufacturing techniques and outperform conventional ones regarding the cost, size, sensitivity, power requirement and dynamic range. Generally, MEMS-based flow sensors are classified as either thermal or non-thermal [1]. The thermal type sensors utilize the heat transfer of fluid flow to modulate the thermal behaviors of sensing elements that can be transduced into electrical signals [2]. The non-thermal type sensors often operate under different principles, such as using lift force, differential pressure, and cantilever deflection [3]–[6]. Recently, graphene has been considered as a suitable material for mechanical sensors due to favorable electrical and mechanical properties. Notably, the piezoresistive effect of graphene caused by strain-induced mechanical-electrical coupling has been reported and utilized for various sensor applications [7]–[9]. Also, because large-area growth and transfer of graphene onto various substrates have been made possible [10], [11], the prospect of merging graphene with sophisticated micromachining techniques opens a promising path to develop graphene-based MEMS mechanical sensors.

In this letter, we present a novel MEMS flow sensor using a suspended graphene diaphragm perforated with microscale air hole arrays. The sensor provides a wide range of 5−56 m/s in velocity, as well as a flow rate sensitivity of $\sim 7 \times 10^{-8} (m/s)^{-1}$.

II. Results and Discussion

The presented flow sensor (Fig. 1a) is formed with a few-layered graphene (∼1 nm thickness) transferred onto the top surface of a 200 nm-thick silicon nitride (Si_3N_4) layer, where a periodic array of microsized through-holes is created (Fig. 1b). The formed graphene-Si_3N_4 composite diaphragm is suspended across over an opening formed in a silicon substrate. As an upward flow passes through the array of holes, a pressure drop will occur between the bottom and top surfaces of the diaphragm, causing deflection of the diaphragm. For example, when an airflow passes through the holes at a flow velocity of 21 m/s, the diaphragm (side length: 490 μm; diameter of air holes: 2.5 μm; period of air holes: 5 μm; hole arrangement: triangular lattice) is deflected by ∼12 μm at its center, as shown by surface profilometry (Fig. 1c). Due to the piezoresistive effect of graphene, the graphene layer changes its resistance. The higher the flow rate, the larger resistance change the graphene has.

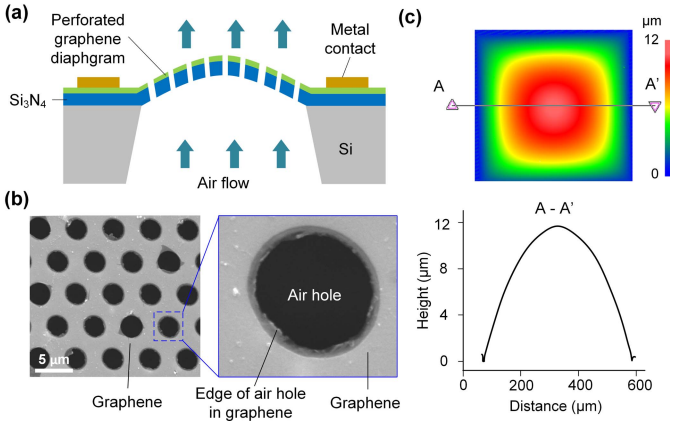

Fig. 1. (a) Schematic of the flow sensor using a suspended graphene-Si3N4 composite diaphragm containing an array of air holes. (b) SEM image showing the graphene sheet containing air holes. The inset shows a close-up of an air hole created in graphene. (c) The upper panel shows the measured surface profile of the suspended diaphragm at a 21 m/s flow velocity of air. The lower panel shows the deflection of the diaphragm along the line A-A'.

To fabricate the sensor, a 200 nm-thick Si_3N_4layer is first deposited onto a double side polished silicon substrate using chemical vapor deposition, followed by forming an array of holes via photolithography and reactive ion etching. An etching window is also opened at the back of the substrate using the same patterning method (Fig. 2a). Following that, the silicon beneath the diaphragm region is etched away using a conventional anisotropic wet etching method, thus realizing a suspended Si_3N_4 membrane (490×490 μm^2) (Fig. 2b). A few-layered, ∼1 nm-thick graphene sheet is then transferred onto the top of the nitride membrane using the method described in [11] (Fig. 2c). The inset of Fig. 2c shows that the transferred graphene can cover the holes in the Si_3N_4 layer. Subsequently, the graphene layer is patterned to obtain a resistor with the help of a shadow mask and oxygen plasma etching. Then, electrical contacts are made by e-beam evaporation of gold with another shadow mask (Fig. 2d). After that, the silicon substrate is flipped over and then adhered to a silicon carrier wafer using photoresist as a temporary adhesive. This allows

Manuscript received June 14, 2018; revised September 7, 2018; accepted September 22, 2018. Date of publication October 19, 2018; date of current version November 29, 2018. This work was supported in part by the United States National Science Foundation under Grants IOS-1650182 and ECCS-1711839 and in part by the Plant Sciences Institute at the Iowa State University. Subject Editor X. Wang. *(Corresponding author: Liang Dong.)*

The authors are with the Department of Electrical and Computer Engineering, Iowa State University, Ames, IA 50011 USA, and also with the Microelectronics Research Center, Iowa State University, Ames, IA 50011 USA (e-mail: ldong@iastate.edu).

Color versions of one or more of the figures in this paper are available online at http://ieeexplore.ieee.org.

Digital Object Identifier 10.1109/JMEMS.2018.2874231

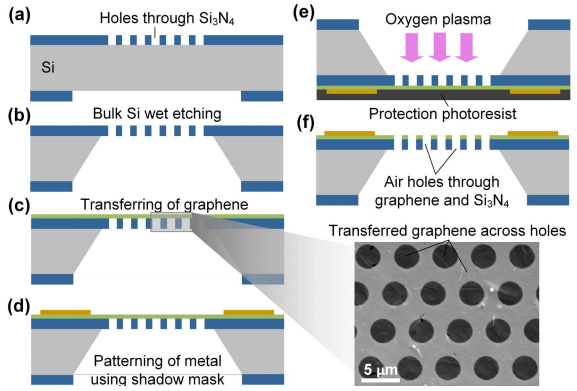

Fig. 2. Brief fabrication process flow for the flow sensor.

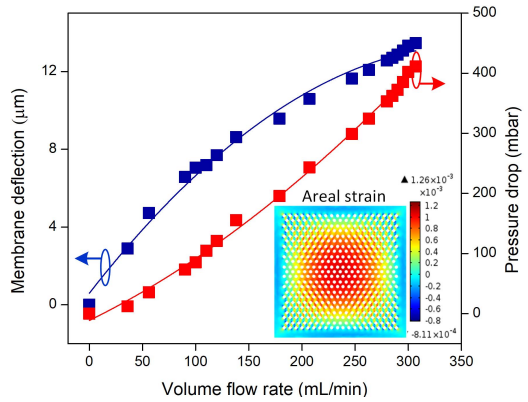

Fig. 3. Measured out-of-plane deflection at the center of the diaphragm (right) and corresponding pressure drop across the diaphragm (left) as a function of flow velocity of air. The inset gives the simulated areal strain distribution over a reduced-length diaphragm under a pressure drop of 400 mbar. The side length of the diaphragm used in the simulation is 200 μm, which is only one half of the length of the fabricated sensor.

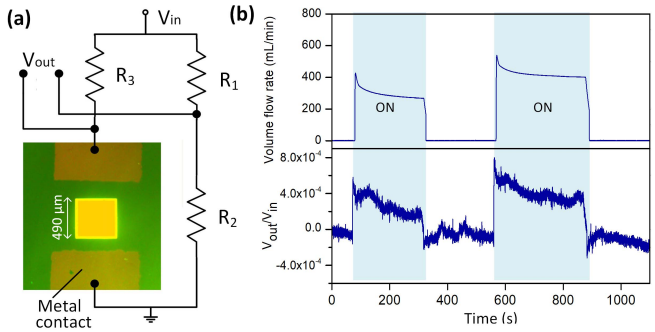

Fig. 4. (a) Optical image of the flow sensor and Wheatstone bridge circuit used to produce voltage output of the sensor. (b) Voltage response of the sensor to different air flow velocities.

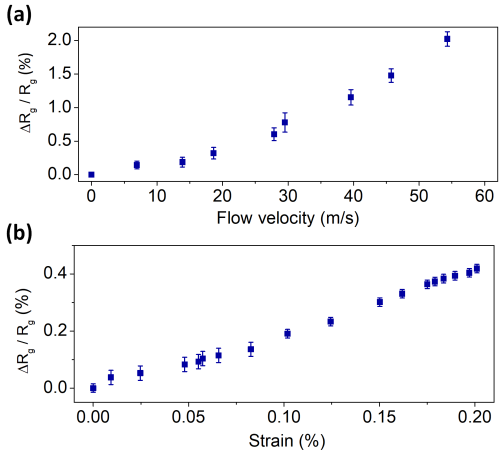

Fig. 5. (a) Measured resistance response from the sensor to different input air flow velocities. (b) Measured resistance responses to different areal strains calculated at the center of the graphene diaphragm when the air flow rate changes from 0 to 22 m/s. COMSOL Multiphysics is used to calculate the areal strain under different input air flow rates.

etching the graphene from the bottom of the holes by oxygen plasma. Here, the perforated Si_3N_4 membrane serves as a shadow mask (Fig. 2e). The holes are thus created in the graphene layer. After the photoresist is removed, the sensor is fabricated (Fig. 2f).

Fig. 3 shows the measured out-of-plane deflection δ at the center of the perforated diaphragm as a function of flow velocity v_{flow} of air. δ is observed to increase with increasing v_{flow}. it is also possible to convert δ to pressure drop P across the diaphragm using the equation [9]: $P = \frac{B_1 t\sigma_0}{(a/2)^2}\delta + \frac{B_2 f(v) tE}{(a/2)^4(1-v)}\delta^3$, where a, $f(v)$ and t represent the side length, geometry function and thickness of the diaphragm, respectively, $B_1 = 3.45$ and $B_2 = 1.994$ are dimensionless constants, $\sigma_0 = 58$ MPa is the initial stress, $E = 239$ GPa is the Young's modulus, and $v = 0.22$ is the Poisson ratio [9]. For $v_{\text{flow}} = 21$ m/s, we obtain $\delta = 12$ μm, corresponding to $P = 400$ mbar. Fig. 3 also shows the pressure drop as a function of v_{flow}. To illustrate the strain distribution across the diaphragm under a stressed condition, a mechanical simulation is performed using COMSOL Multiphysics®. Due to limited computational power, the simulation uses a reduced model for the square diaphragm with a side length of 200 μm. Under a 400 mbar pressure drop, the reduced-length diaphragm shows a maximum areal strain of 0.126% at its center and a deflection of 3.34 μm (see the inset in Fig. 3).

Fig. 4b shows the dynamic response of the sensor to changing flow rate of air passing through the microholes. A Wheatstone bridge circuit (Fig. 4a) determines the sensor output, where $V_{\text{in}} = 10$ mV, $R_1 = R_2 = 300$ Ω, and R_3 is adjusted to match the total resistance of graphene $R_{\text{total}} = 275$ Ω. When a step-like flow rate is applied, the output voltage immediately changes, indicating the instant response of the sensor to an input airflow. Also, over the testing period, the pattern of the output voltage almost follows that of the input flow rate.

Fig. 5a shows the static resistance response of the sensor to different input flow rates of air from 0 to 56 m/s. As the flow rate increases, the resistance of the sensor increases. Based on the noise floor at the output of the sensor (Fig. 4b), the noise equivalent flow rate of the sensor is ~2.4 m/s. In addition, by taking the measurement error of ~2.6 m/s into consideration, the minimum detectable flow rate is found to be ~5 m/s. Therefore, the dynamic range of the sensor is 5–56 m/s. The overall sensitivity of the sensor is estimated as $V_{\text{out}}/(V_{\text{in}} \cdot v_{\text{flow}}) = \sim 7\times10^{-8}$ $(\text{m/s})^{-1}$ by averaging all the sensitivities calculated from the measurement results shown in Fig. 4b. It should be noted that the noise level of the sensor is considerably high, compared to the output voltage. Thermal noise is unavoidable background noise of the sensor. Heat generation due to current flow in the sensor is another source of the noise. In addition, environmental mechanical vibration may cause extra noise. Non-inert molecules or moisture in the air could also be directly absorbed on the graphene and perturb the measurement result [8]. The overall noise level could be reduced by optimizing the readout circuit, e.g., using a high-performance low-pass filter and a low-noise amplifier. It is noteworthy that because the surface of the nitride membrane is treated with oxygen plasma prior to transferring the graphene layer onto the

TABLE I

PERFORMANCE COMPARISON BETWEEN VARIOUS MEMS FLOW SENSORS

Device structure and principle	Device parameters			
	Size (μm^2)	Dynamic range (ms^{-1})	Resolution of detection (ms^{-1})	Refs
Perforated graphene (piezoresistive)	490×490	5–56	5	This work
Paddle (piezoresistive)	300×1500	0–29	2	3
Paddle (capacitive)	100×100	2–16	0.5	12
Mo wires (thermoresistive)	350×54	0-26	< 0.1	13
Pillar (optical)	2000×23	0.03–0.15	0.01	14

nitride layer, the binding between the graphene and nitride layers is improved and no delamination of graphene is observed. Further, Fig. 5b plots the measured resistance change of the graphene layer containing the microhole array as a function of areal strain at the center of the diaphragm for different input flow rates of air up to 22 m/s.

Table 1 compares our device with other MEMS flow sensors. While point-to-point comparisons between various sensors are almost impossible due to using different sensing principles and readout circuits, our sensor is advantageous over other sensors in terms of detection range and relatively simple fabrication process. It should be pointed out that the current design uses the 490 μm-side length diaphragm and 2.5 μm-diameter microholes. This configuration has much room to improve for higher sensitivity, more extensive detection range, and better mechanical robustness. Given an input flow rate or a pressure drop across the diaphragm, the larger the surface area of the diaphragm, the more deflection the diaphragm will provide, and thus, the higher sensitivity the sensor will exhibit. However, increasing the diaphragm area may risk mechanical failure of the device, because the large diaphragm will have a high chance to crack or even pop out due to an increased deflection. Lastly, to measure flow rates of other gases (e.g., argon, oxygen, nitrogen) than air at different temperatures, the sensor should be carefully calibrated, because some non-inert molecules could be directly absorbed on graphene [8], thus perturbing the intrinsic resistance change of graphene in addition to the piezoresistive effect. Therefore, our future work will include optimizing the sensor structure (e.g., diaphragm area and thickness, air hole diameter and filling factor, graphene sheet thickness, etc) and the readout circuit (e.g., reducing noise) to improve sensor performances and explore new applications.

III. CONCLUSION

In summary, we have developed a small footprint graphene-based MEMS flow sensor. The graphene-Si_3N_4 composite diaphragm with an array of air holes allows passing airflow through the perforated diaphragm and converts the airflow-induced mechanical deflections to electrical resistance changes. The creation of the unique microscale hole array allows for a wide dynamic flow velocity range of 5−56 m/s with the overall sensitivity of $\sim 7\times10^{-8}(\mathrm{m/s})^{-1}$.

REFERENCES

[1] J. T. W. Kuo, L. Yu, and E. Meng, "Micromachined thermal flow sensors-a review," *Micromachines*, vol. 3, no. 3, pp. 550–573, Mar. 2012.

[2] Y.-H. Wang *et al.*, "MEMS-based gas flow sensors," *Microfluidics Nanofluidics*, vol. 6, no. 3, pp. 333–346, Jan. 2009.

[3] V. K. Agrawal, R. Patel, D. Boolchandani, and K. Rangra, "Analytical modeling, simulation, and fabrication of a MEMS rectangular paddle piezo-resistive micro-cantilever-based wind speed sensor," *IEEE Sensors J.*, vol. 18, no. 18, pp. 7392–7398, Sep. 2018.

[4] Q. Zhang, W. Ruan, H. Wang, Y. Zhou, Z. Wang, and L. Liu, "A self-bended piezoresistive microcantilever flow sensor for low flow rate measurement," *Sens. Actuators A, Phys.*, vol. 158, no. 2, pp. 273–279, Mar. 2010.

[5] N. Svedin, E. Kalvesten, and G. Stemme, "A new edge-detected lift force flow sensor," *J. Microelectromech. Syst.*, vol. 12, no. 3, pp. 344–354, Jun. 2003.

[6] M. Rajavelu, D. Sivakumar, R. J. Daniel, and K. Sumangala, "Perforated diaphragms employed piezoresistive MEMS pressure sensor for sensitivity enhancement in gas flow measurement," *Flow Meas. Instrum.*, vol. 35, pp. 63–75, Mar. 2014.

[7] K. S. Kim *et al.*, "Large-scale pattern growth of graphene films for stretchable transparent electrodes," *Nature*, vol. 457, no. 7230, pp. 706–710, Feb. 2009.

[8] S.-E. Zhu, M. K. Ghatkesar, C. Zhang, and G. C. A. M. Janssen, "Graphene based piezoresistive pressure sensor," *Appl. Phys. Lett.*, vol. 102, no. 16, p. 161904, Apr. 2013.

[9] Q. Wang, W. Hong, and L. Dong, "Graphene 'microdrums' on a free-standing perforated thin membrane for high sensitivity MEMS pressure sensors," *Nanoscale*, vol. 8, no. 14, pp. 7663–7671, Mar. 2016.

[10] A. Reina *et al.*, "Large area, few-layer graphene films on arbitrary substrates by chemical vapor deposition," *Nano Lett.*, vol. 9, no. 1, pp. 30–35, Jan. 2009.

[11] J. W. Suk *et al.*, "Transfer of CVD-grown monolayer graphene onto arbitrary substrates," *ACS Nano*, vol. 5, no. 9, pp. 6916–6924, Sep. 2011.

[12] S. D. Nguyen, I. Paprotny, P. K. Wright, and R. M. White, "In-plane capacitive MEMS flow sensor for low-cost metering of flow velocity in natural gas pipelines," in *Proc. IEEE 27th Int. Conf. Micro Electro Mech. Syst. (MEMS)*, Jan. 2014, pp. 971–974.

[13] M. Ahmed, W. Xu, S. Mohamad, M. Duan, Y.-K. Lee, and A. Bermak, "Integrated CMOS-MEMS flow sensor with high sensitivity and large flow range," *IEEE Sensors J.*, vol. 17, no. 8, pp. 2318–2319, Apr. 2017.

[14] J. Paek and J. Kim, "Microsphere-assisted fabrication of high aspect-ratio elastomeric micropillars and waveguides," *Nature Commun.*, vol. 5, Feb. 2014, Art. no. 3324.